Key Engineering Materials
ISSN: 1662-9795, Vol. 926, pp 288-296
doi:10.4028/p-kf8tl3

Submitted: 2021-12-07
Accepted: 2022-03-08
Online: 2022-07-22

Metamaterial Mechanical Performances: A Single Cell Analysis

Ranzini G.[1,a], Giorleo L.[1,b*] and Ceretti E.[1,c]

[1]Departement of Mechanical and Industrial Engineering, University of Brescia, Italy

[a]g.ranzini@unibs.it, [b]luca.giorleo@unibs.it, [c]elisabetta.ceretti@unibs.it

Keywords: Metamaterials; Design for Additive; Mechanical Behaviour

Abstract. In this research the effect of the geometric features of an auxetic metamaterial structure was investigated by the authors. In particular, a re-entrant honeycomb geometry was selected as case study. Connectors inclination, width and length have been changed to study mechanical behavior and deformation under compression. The procedure adopted was both experimental and numerical. Solutions proposed highlight benefits in terms of compression load and controlled lateral displacement that is possible to achieve.

Introduction

Additive manufacturing is an enabling technology of Industry 4.0 thanks to its ability to produce parts characterized by complex structure [1-2]. This ability let the possibility to redesign not only the shape of the part but also to rethink about the chance to do not produce parts as full but with hierarchical structures [3-4]. It is also possible to redesign objects in a single part so that it is avoided the assembly step. In addition, not being a subtractive method, it helps to not waste material [5-6]. In particular, different researches are now focusing on the idea of integrating the concept of metamaterials (materials with a property that is not found in nature) in part geometry to enhance mechanical properties and weight reduction [7-8]. Their most distinguishing feature is that their macroscopic behaviour is not related to the molecular structure but to the cells geometry that makes up the part [8]. There are two different kind of metamaterials: Auxetic and Non Auxetic. The first one presents the Poisson Coefficient negative while the second one has it positive. In this way, the Auxetic object, under a traction load, expands its transversal section instead of shrinking it (Figure 1.a). Thanks to this particular property there are several application fields that are interested in: medical, acoustic, aerospace, sensors and actuators [9-10]. Another kind of Auxetic structure is the so called Chiral: this type of material does not have a centre of symmetry and the cells are created by connecting ligaments to a node. In this case, the mono axial load causes the rotation of the nodes and consequently the deformation of the ligaments attached to (Figure 1.b). It is also possible to create rigid rotating structures by connecting the cells only in their vertexes. In this way, when these structures are stretched, the solids rotate around the pivots resulting in an expansion in both directions (Figure 1.c) [11-12].

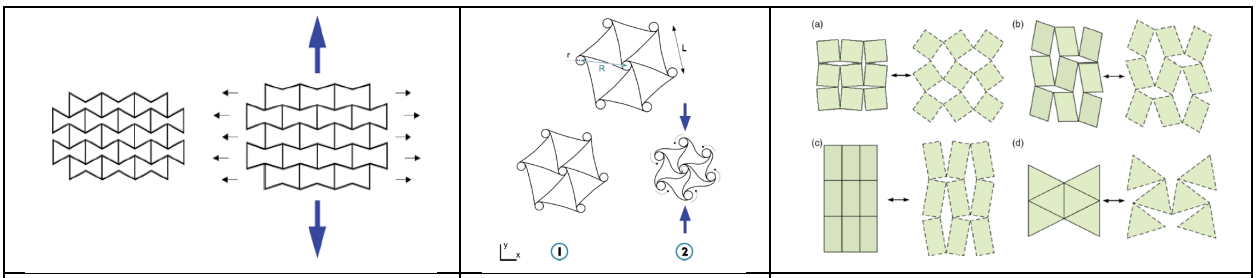

(a)	(b)	(c)

Figure 1: Auxetic (a), chiral (b) and pivots (c) metamaterials design. [8]

However, an important feature about metamaterials is the capability of realizing mechanisms by only using the deformation of the auxetic structures; in this case an important role to control the movement is the control of the geometric features that define the single cell design. In order to enlarge the knowledge about this topic in this research, the authors investigated the effect of the geometric

features of an Auxetic metamaterial structure. In particular, a re-entrant honeycomb geometry was selected as case study. Connector's inclination, width and length have been changed to study the mechanical behaviour and the deformation under compression. Finally, the authors propose a new geometry cell able to control the cell deformation.

Materials and Methods

In this study a re-entrant honeycomb geometry was selected as a demonstrator. The starting cell geometry design is presented in Figure 2.a and Table 1.

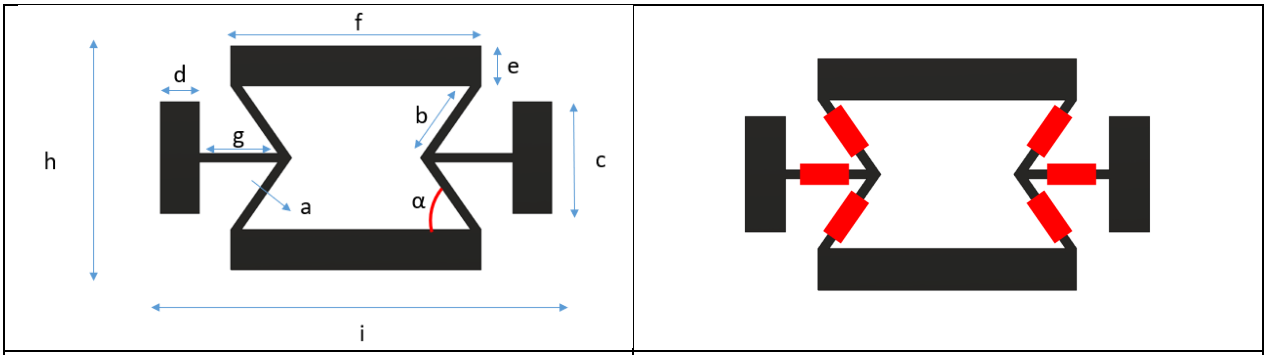

(a) (b)

Figure 2: Original (a) and new (b) re-entrant honeycomb cell geometry.

Table 1: Values of the design parameters of the original cell [mm].

a	b	c	d	e	f	g	h	i	t	α
0.8	7	10	3.5	3.6	22.4	7	20	35	3	55°

In the first numerical analysis it has been evaluated the influence of reinforcements design in terms of length and thickness. To manage this task, four different configurations have been proposed to simulate the effect of length and thickness reinforcement variation, two level have been set for each parameter. All the reinforcements were located starting from the middle point of the re-entrant edges of the cell as reported in figure 2.b. The reinforcement follows an increment rule: the length was set equal to the 25% of the length of the re-entrant edges (b value in figure 2.a and table 1) and subsequently by 50%. For the reinforcement thickness level has been chosen in order to increase cell thickness (a value in figure 2.a and Table 1) of 25% and 50% respectively. Table 2 shows the process parameters tested. Best results have been choose as starting geometry for the second numerical analysis

Table 2: Reinforcement geometry parameters of the first campaign.

Configurations	1	2	3	4
Length [mm]	1.75	1.75	3.5	3.5
Thickness [mm]	0.4	0.8	0.4	0.8
Length respect to b [%]	25	25	50	50
Thickness respect to a [%]	50	100	50	100

In the second numerical analysis it has been investigated the influence of the fillet radius and its position. The values that were chosen for the fillet radius were equal to 1.6 mm for the external configuration and 0.4 mm for the internal one. This was to maintain constant the thickness of the walls around the corners. The analysis investigates about the effect of external or internal fillet radius on the cell deformation behaviour. In the third campaign it was evaluated, based on best configuration of second numerical analysis, the influence of the internal angles (α) of the re-entrant edges. Two different values have been chosen: 40° and 70°.

In all numerical analysis the cells have been designed and numerically analysed in Fusion 360, an Autodesk Software. The numerical simulations have been set as following: it was imposed a downward displacement of 3 mm of the upper crossbar of the cell while keeping the lower one fixed. In this way it has been possible to evaluate the compression load needed to lower the crossbar by 3 mm. In addition to the compression load, the stresses and the lateral displacement of the structure can be calculated too. The material mechanical behaviour simulated is coherent with the material used for the experimental analysis reported in Table 3.
The most interesting results have been experimentally tested. The structures were realized in Onyx by Fused Filament Fabrication (FFF) method with a Markforged Desktop Two. The material was provided by Markforged and it consisted in Nylon added with micro carbon fibres. The mechanical properties of Onyx are shown in Table 3.

Table 3: Onyx mechanical properties.

Properties	Onyx
Tensile Modulus (GPa)	2.4
Tensile Strength (MPa)	40
Tensile Stress at Break (MPa)	37
Tensile Strain at Break (%)	25
Flexural Modulus (GPa)	3
Flexural Strength (MPa)	71
Density (g/cm³)	1.2

The case studies produced have been tested with a bench vice imposing a displacement coherent with the simulation and analysing the results from a qualitative point of view.

Results

Simulation of original geometry

To compare the results of the numerical analysis in this section the simulation results of the original cell geometry are presented. As reported in figure 3.a, the load needed to induce a displacement of 3 mm was equal to 158 N and the higher stress is equal to 230 MPa and is located on the cell knee. In addition, it has been evaluated the lateral displacement of the re-entrant honeycomb structure. The points that have been individuated for investigating the lateral movement along the x axis, for every configuration made, are shown in Figure 3.b. How it can be seen, there was a great difference between the upper and the lower corner displacement of the right box attached to the cell. The upper corner displacement it is equal to 1.73 mm while the lower corner displacement is about 2.08 mm.

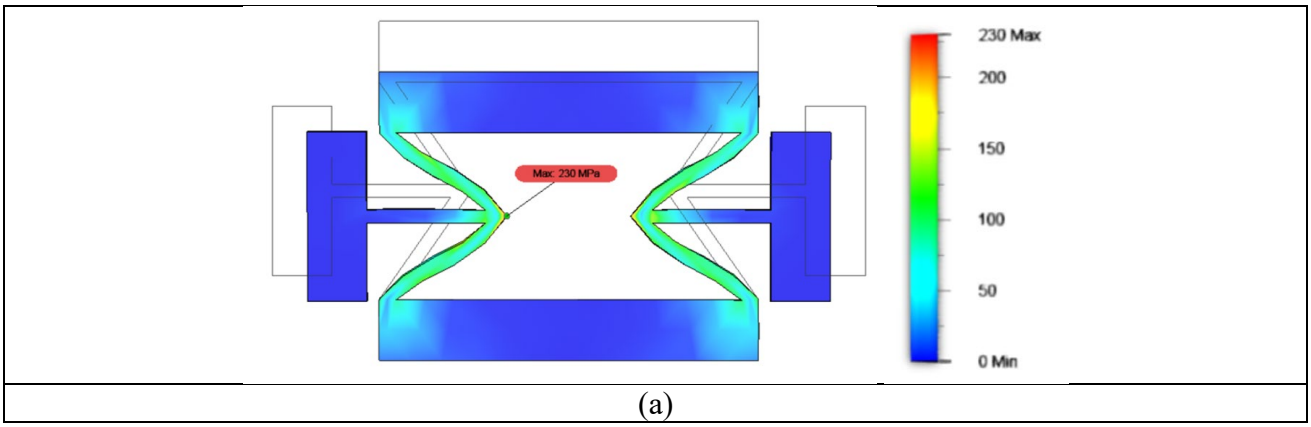

(a)

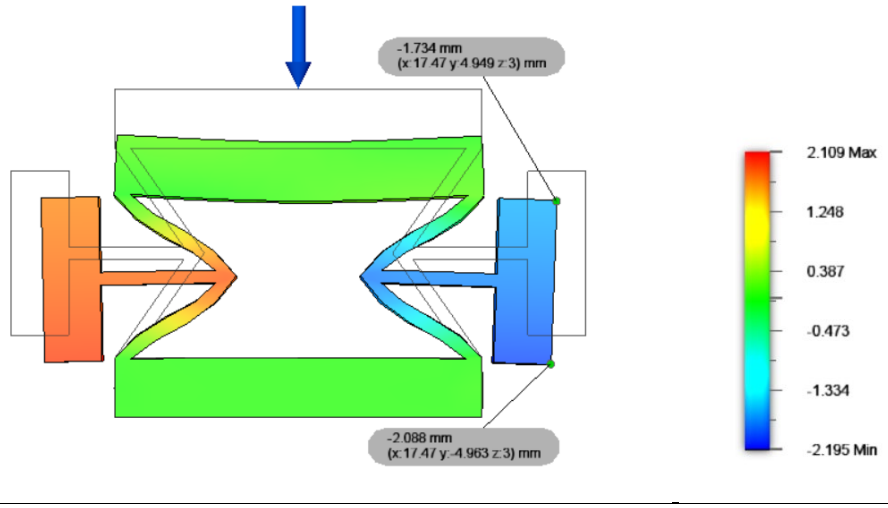

(b)

Figure 3: Stress analysis (a) and lateral displacement (b) of the original configuration

First experimental analysis: effect of reinforcement geometry

In the Table 4 it is possible to see a summary of stress and displacement analysis of the whole set of simulations.

Table 4: Load, maximum stress and lateral displacement estimated.

Configurations	Load [N]	Maximum Stress [MPa]	X displacement [mm]	Z displacement [mm]
original	158	229	0.35	0.45
1	92	224	0.14	0.05
2	112	225	0.22	0.04
3	98	256	0.12	0.03
4	107	230	0.15	0.10

How it is clear from the obtained data, the presence of the reinforcement and its length and width had an influence on the maximum stress that occurred in the structure. Starting from the original unreinforced cell that needed 158 N, all the other simulations with reinforcements showed a lower values of compression load. In addition, comparing 1 to 2 and 3 to 4, where the only change is the reinforcement width (3 and 4 +50% than 1 and 2), it possible to see that the compression load increased by 22% and 9% respectively. Comparing 1 to 3 and 2 to 4, where the only change is the reinforcement length (3 and 4 +25% than 1 and 2), it is evident that the structures with the longer reinforcement require a bigger force. Regarding the stresses, a significant difference compared to the original structure except for a +12% in simulation 3 can be obtained. About lateral displacement, the presence of the reinforcements reduces lateral displacement from 0.45 to 0.03 mm along z axis and from 0.35 to 0.12 mm along x axis adopting configuration 3. Similar results are achieved using configuration 1.

Comparing the results obtained and giving a higher priority to load and stress optimization, the best compromise between compression load, maximum stress and lateral displacement values has been individuated in the configuration 1. In Figure 4 a comparison between original and configuration 1 is presented as a function of stress (figure 4.a and 4.b) and lateral displacement (figure 4.c and 4.d).

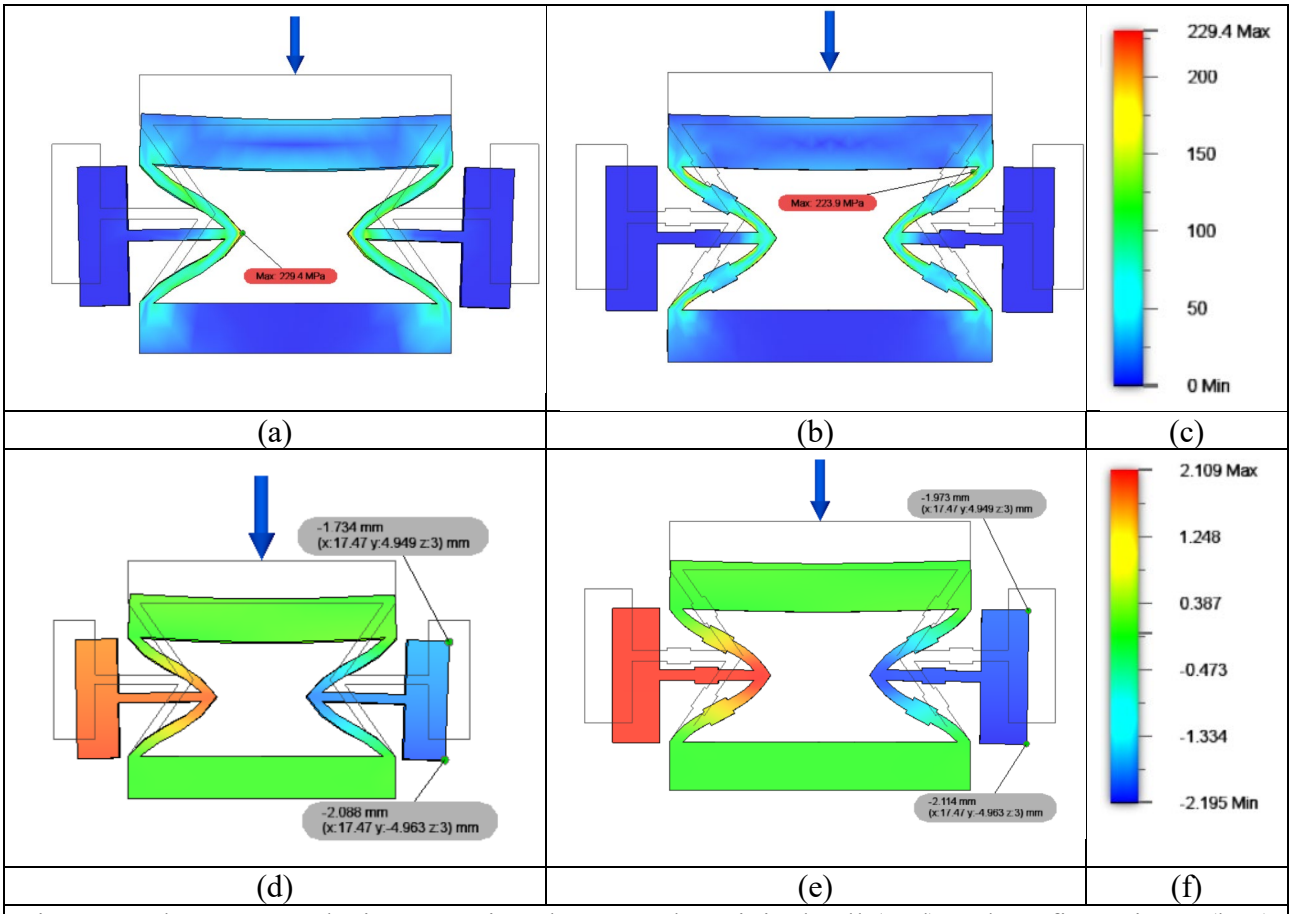

(a) (b) (c)

(d) (e) (f)

Figure 4: The stress analysis comparison between the original cell (a, d) and configuration 1 (b, e) and relative scale bar (c, f).

Second experimental analysis: effect of filler radius

In this analysis, the influence of the fillet radius on the cell deformations and stresses of the configuration 1 has been evaluated. Table 5 shows main results.

Configurations	Load [N]	Maximum Stress [MPa]	X displacement [mm]	Z displacement [mm]
1	92	224	0.15	0.05
External	88	233	0.11	0.06
Internal	130	446	0.12	0.05

Table 5: Load, maximum stress and lateral displacement estimated.

When the internal radius is filleted there was an increase of material in the cell knees of the structure and thus, using the same amount of force of the not filleted configuration (92N), it was reached a lowering of the upper crossbar by 2 mm instead of 3 mm. With external fillet radius (Figure 7), it was observed the opposite effect. With a force equal to 88 N, lower than in simulation 1, it was obtained a crossbar displacement of 3 mm. On the other hand, it was reached a higher stress value of 233 MPa. Regarding the lateral movement along the x axis, there was an improvement: the difference between the upper and the lower corner of the aside box is equal to 0.11 mm. In addition, the deformation along the z axis, is approximately the same as the previous configuration, in fact its value is equal to 0.06 mm.

Based on this analysis and taking into account the importance of fillet radius to avoid crack generation phenomena, the authors selected the configuration external as the optimum. Figure 5 presents the comparison between configuration 1 and external.

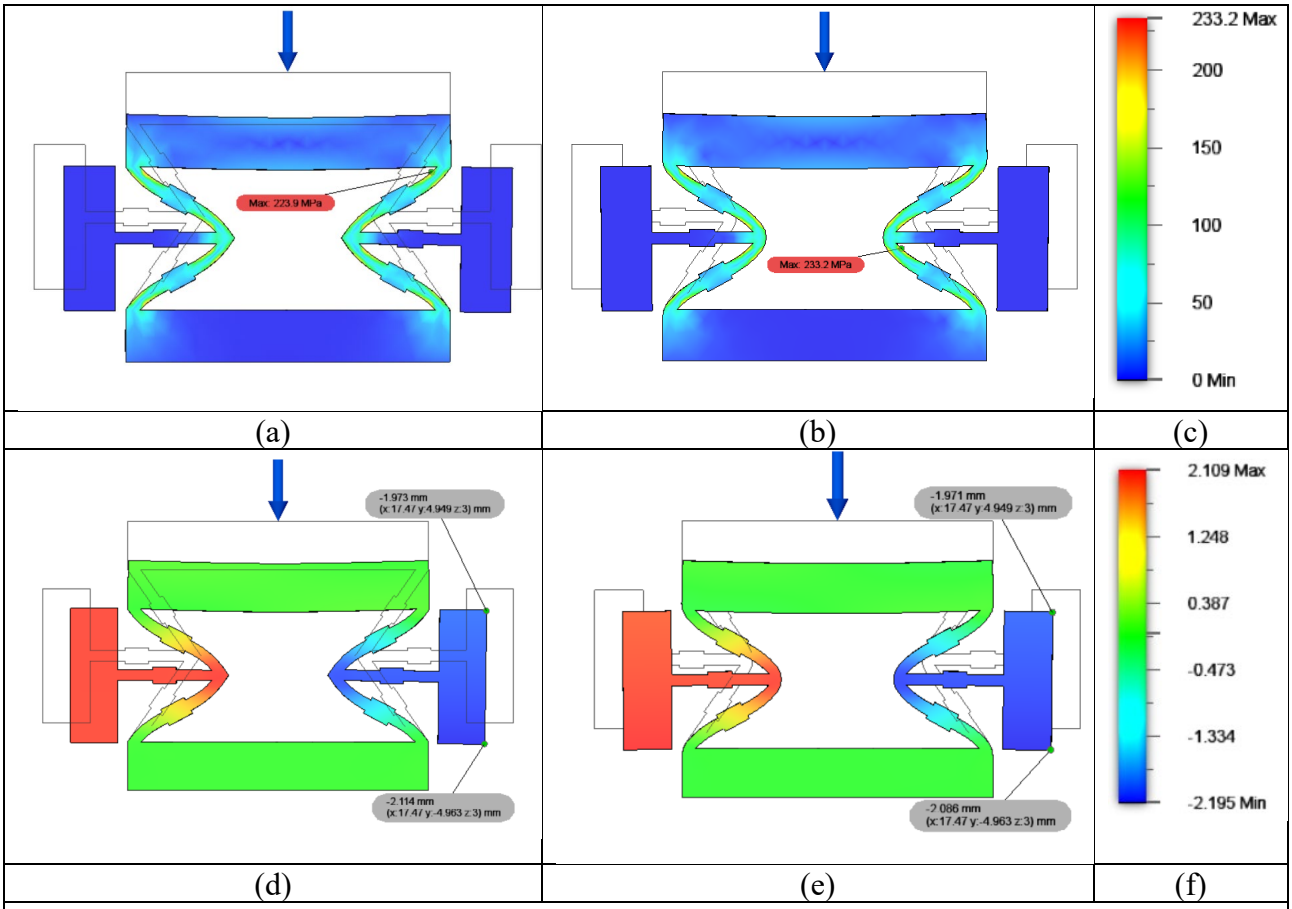

(a) (b) (c)

(d) (e) (f)

Figure 5: The stress analysis comparison between the configuration 1 (a, d) and configuration external (b, e) and relative scale bar (c, f).

Third experimental analysis: effect of reinforcement inclination

In this section, using the first configuration with external fillet radius, the impact of the internal angles (α) on the loads, stresses and displacements that could occur in the structure was investigated. The two values that were chosen are: 70° and 40°. Main results are presented in Table 7.

Table 7: Comparison between the external cell and configurations with different α.

Configurations	Load [N]	Maximum Stress [MPa]	X displacement [mm]	Z displacement [mm]
external (α = 55°)	88	233	0.11	0.06
α = 70°	319	487	0.681	0.09
α = 40°	26	106	0.03	0.02

With an internal angle of 70° it is necessary a higher compression force to obtain a 3 mm displacement of the upper crossbar compared to the 55° cell. In fact, there were needed 319 N to obtain the same vertical displacement. In addition, the stress increased to 487 MPa. The difference between the upper and the lower corners of the aside box was relevant: 0.681 mm. Also the deformation along the z axis rose to 0.09 mm. On the other hand, a cell with an internal angle of 40° needed a 26 N force to be compressed by 3 mm with a very low stress: 106 MPa. In addition, in contrast to the 70° configuration, the movement along the x axis is more homogeneous. The difference between the upper and the lower corners of the aside box is about 0.03 mm. Regarding the deformation along the z axis, a good behaviour with a maximum value of 0.02 mm was obtained.

Displacement Control

To set a limit on the lateral displacement of the re-entrant honeycomb structure a triangular shape on the aside box was designed as it is shown in Figure 8. By editing the inclination of the new edges, it is possibly to define the lateral movement. Therefore, in all the previous situations, the force drove the displacements while in this case the displacement is limited by the new supports.

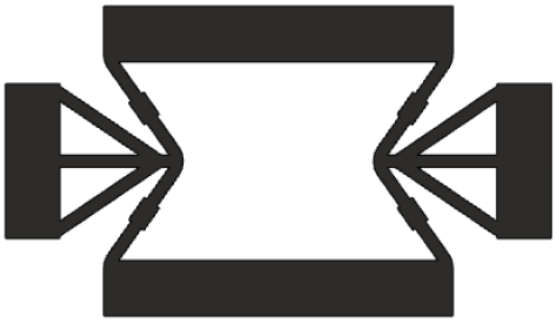

Figure 8: The configuration with the structural control of the lateral displacement.

In addition to the displacement control, the new triangular shape helps to reduce the maximum stress that occur in the structure. By applying the 88 N load, the one of the external fillet radius configuration, a stress value of 228 MPa, with a 3% decrease was obtained. The lateral movement, instead, had no significant variation as can be seen in Table 8. In Figure 9 it is possible to see a simulation of the comparison between the external filleted radius with new triangular configuration.

Table 8: Comparison between the external cell and the triangular design shape.

Configurations	Load [N]	Maximum Stress [MPa]	X displacement [mm]	Z displacement [mm]
external ($\alpha = 55°$)	88	233	0.11	0.06
Triangular	88	228	0.12	0.05

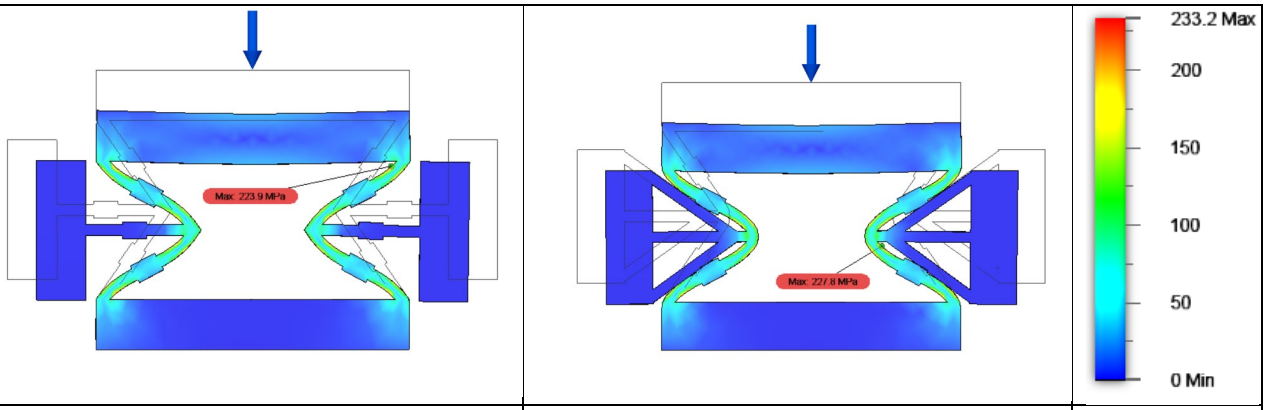

(a) (b) (c)

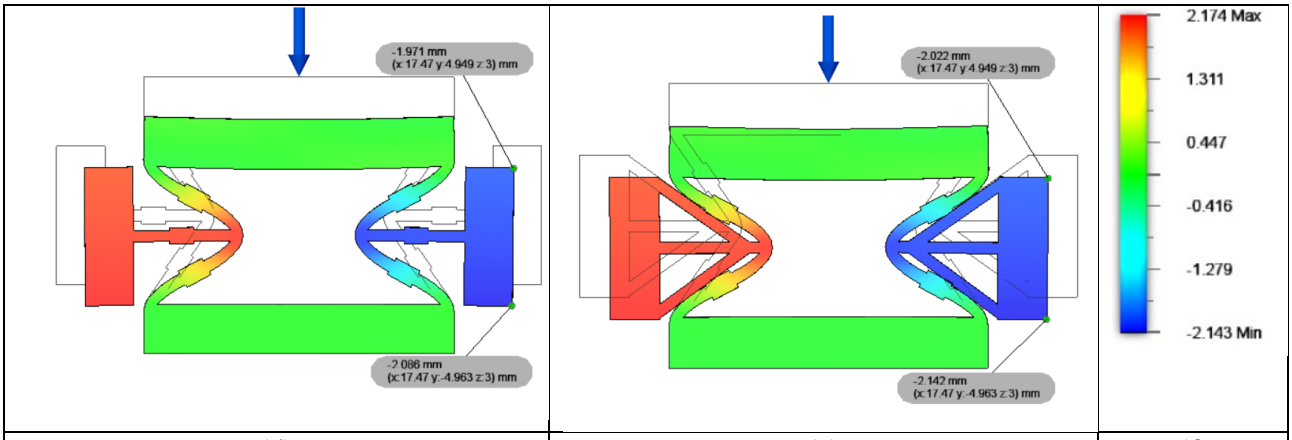

(d) (e) (f)

Figure 9: The stress analysis (a) and (b) and the relative scale bar (c), in (d) and (e) the lateral displacement analysis.

Experimental validation

Few configurations have been tested and confirmed what had been found in numerical simulations. Regarding the geometry of simulation 1 and the external fillet radius, even in this case a good match with the numerical simulation was obtained, avoiding the crack and the deformation along the z direction (Figure 10)

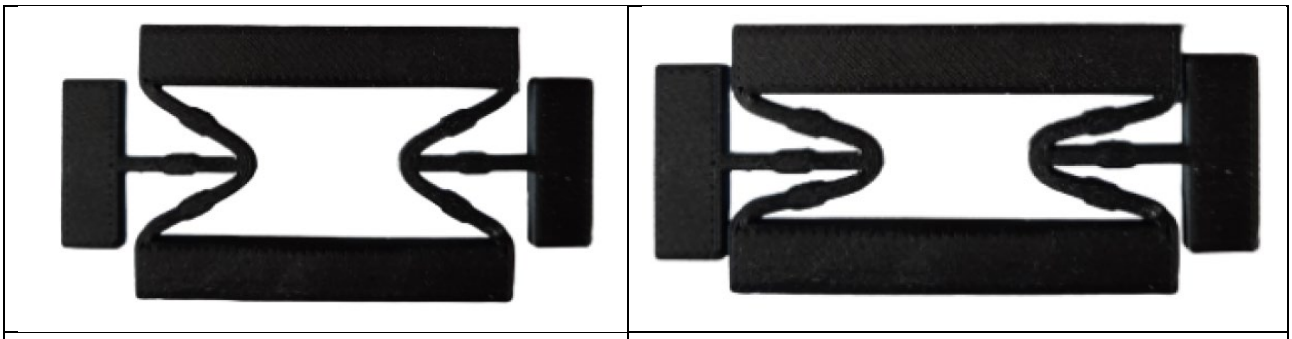

(a) (b)

Figure 10: In (a) the printed cell before the compression and in (b) after the compression.

The last geometry tested was the one with displacement control made by the triangle obstacle on the aside box (Figure 11).

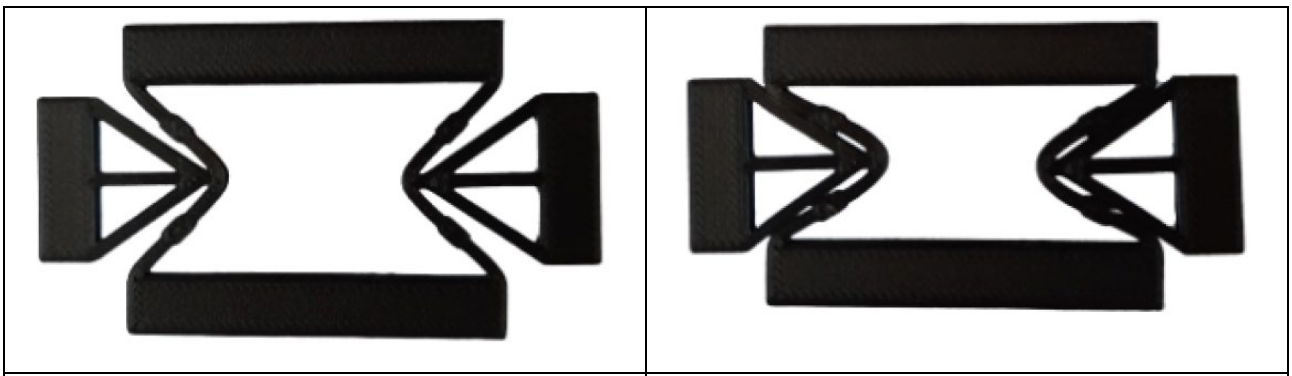

(a) (b)

Figure 11: In (a) un the structure before the compression, in (b) after the compression.

Conclusions

In this research the analysis of geometrical feature on an auxetic metamaterial cell was investigated. Results highlight how increasing thickness of connector, introduce a fillet radius or modify cell inclination could significantly affect the load needed to impose a displacement, the stress undergone and the amount of lateral deformation. In particular, the authors found good results in terms of load and maximum stress reduction when the cell has: a connector with a core thickness increased by 50%; an external fillet radius equal to the connector thickness; a connector inclination equal to 40°. Moreover, the authors introduced a different cell geometry with triangular features on the cell side to control the deformation. A quantitative comparison was finally realized with experimental tests. Future activities are ongoing to investigate the mechanical behaviour of cells array.

References

[1] Ngo, T.D., Kashani, A., Imbalzano, G., Nguyen, K.T.Q., Hui, D. Additive manufacturing (3D printing): A review of materials, methods, applications and challenges (2018) Composites Part B: Engineering, 143, pp. 172-196. DOI: 10.1016/j.compositesb.2018.02.012

[2] Gao, W., Zhang, Y., Ramanujan, D., Ramani, K., Chen, Y., Williams, C.B., Wang, C.C.L., Shin, Y.C., Zhang, S., Zavattieri, P.D. The status, challenges, and future of additive manufacturing in engineering (2015) CAD Computer Aided Design, 69, pp. 65-89. DOI: 10.1016/j.cad.2015.04.001

[3] Giorleo, L., Tegazzini, F., Sartore, L. 3D printing of gelatin/chitosan biodegradable hybrid hydrogel: Critical issues due to the crosslinking reaction, degradation phenomena and process parameters (2021) Bioprinting, 24, art. no. e00170. DOI: 10.1016/j.bprint.2021.e00170

[4] Giorleo, L., Bonaventi, M., Casting of complex structures in aluminum using gypsum molds produced via binder jetting (2021) Rapid Prototyping Journal, 27 (11), pp. 13-23, DOI: 10.1108/RPJ-03-2020-0048

[5] Razavi, S.M.J., Avanzini, A., Cornacchia, G., Giorleo, L., Berto, F., Effect of heat treatment on fatigue behavior of as-built notched Co-Cr-Mo parts produced by Selective Laser Melting (2021) International Journal of Fatigue, 142, art. no. 105926, DOI: 10.1016/j.ijfatigue.2020.105926

[6] Tomasoni, D., Colosio, S., Giorleo, L., Ceretti, E., Design for additive manufacturing: Thermoforming mold optimization via conformal cooling channel technology (2020) Procedia Manufacturing, 47, pp. 1117-1122. DOI: 10.1016/j.promfg.2020.04.128

[7] Kolken, H.M.A., Zadpoor, A.A. Auxetic mechanical metamaterials (2017) RSC Advances, 7 (9), pp. 5111-5129, DOI: 10.1039/c6ra27333e

[8] Yang, Y. Sun and T. C. Lueth, "Construction of a Production Line for Auxetic Structures Using Novel Modelling Method*," 2019 IEEE International Conference on Robotics and Biomimetics (ROBIO), 2019, pp. 1627-1632, doi: 10.1109/ROBIO49542.2019.8961614

[9] Tan, T. W., Douglas, G. R., Bond, T., and Phani, A. S. (November 7, 2011). "Compliance and Longitudinal Strain of Cardiovascular Stents: Influence of Cell Geometry." ASME. J. Med. Devices. December 2011; 5(4): 041002. DOI: 10.1115/1.4005226

[10] Wang, Z., Luan, C., Liao, G., Liu, J., Yao, X. and Fu, J. (2020), Progress in Auxetic Mechanical Metamaterials: Structures, Characteristics, Manufacturing Methods, and Applications. Adv. Eng. Mater., 22: 2000312., DOI: 10.1002/adem.202000312

[11] Alexandra Ion, Johannes Frohnhofen, Ludwig Wall, Robert Kovacs, Mirela Alistar, Jack Lindsay, Pedro Lopes, Hsiang-Ting Chen, and Patrick Baudisch. 2016. Metamaterial Mechanisms., 529–539. DOI: 10.1145/2984511.2984540

[12] Zhichao Dong, Ying Li, Tian Zhao, Wenwang Wu, Dengbao Xiao, Jun Liang,Experimental and numerical studies on the compressive mechanical properties of the metallic auxetic reentrant honeycomb, Materials & Design, Volume 182, 2019, 108036, DOI: 10.1016/j.matdes.2019.108036